SILVA FENNICA

Silva Fennica 43(2) research articles

www.metla.fi/silvafennica · ISSN 0037-5330
The Finnish Society of Forest Science · The Finnish Forest Research Institute

Exploration of Fracture Dynamics Properties and Predicting Fracture Toughness of Individual Wood Beams Using Neural Networks

Sandhya Samarasinghe

Samarasinghe, S. 2009. Exploration of fracture dynamics properties and predicting fracture toughness of individual wood beams using neural networks. Silva Fennica 43(2): 275–289.

In this study, the time to crack initiation (T_{init}), duration of crack propagation (T_{frac}), crack initiation stress, peak stress as well as crack speed and fracture toughness were investigated for three Rates of Loading (ROL) and four sizes of notched wood beams using high-speed video imaging and neural networks. T_{init} was consistent for all volumes and the average T_{init} was nonlinearly related to volume and ROL. For the smallest ROL, there was a distinct volume effect on T_{init} and the effect was negligble at the largest ROL. However, the stress at crack initiation was not consistent. Contrasting these, T_{frac} for all volumes appeared to be highly variable but the peak stress carried prior to catastrophic failure was consistent. The crack propagation was a wave phenomenon with positive and negative (crack closure) speeds that varied with the ROL. As accurate estimation of crack initiation load (or stress) and its relationship to peak load (or stress) is important for determining fracture toughness, Artificial Neural Networks (ANN) models were developed for predicting them from volume, Young's modulus, face and grain angles, density, moisture content and ROL. Models for crack initiation load and peak load showed much higher predictive power than those for the stresses with correlation coefficients of 0.85 and 0.97, respectively, between the actual and predicted loads. Neural networks were also developed for predicting fracture toughness of individual wood specimens and the best model produced a statistically significant correlation of 0.813 between the predicted and actual fracture toughness on a validation dataset. The inputs captured 62% of variability of fracture toughness. Volume and Young's modulus were the top two contributing variables with others providing lesser contributions.

Keywords cracks, initiation, New Zealand, peak stress, *Pinus radiata*, speed, video imaging, wood properties
Addresses Centre for Advanced Computational Solutions (C-fACS), Lincoln University, Canterbury, New Zealand
E-mail sandhya.samarasinghe@lincoln.ac.nz
Received 31 December 2007 **Revised** 6 April 2009 **Accepted** 21 April 2009
Available at http://www.metla.fi/silvafennica/full/sf43/sf432275.pdf

Symbols

a	=	crack length
b	=	thickness of specimen
h	=	height
L	=	span
P	=	applied load
P_{init}	=	crack initiation load
P_{peak}	=	peak load
LR	=	Longitudinal-Radial plane
LT	=	Longitudinal-Tangential plane
K_{Ic}	=	Mode-I fracture toughness
$K_{Ic(LR)}$	=	Mode-I fracture toughness (crack perpendicular-to-grain and propagating in radial direction)
$K_{Ic(LT)}$	=	Mode-I fracture toughness (crack perpendicular-to-grain and propagating in tangential direction)
$K_{Ic(TL)}$	=	Mode-I fracture toughness (crack perpendicular to tangential direction and propagating in longitudinal direction)
$G_{Ic(TL\ or\ RL)}$	=	Mode-I critical energy release rate
T_{init}	=	time to crack initiation
T_{frac}	=	duration of crack propagation
ANN	=	Artifical Neural Networks
DOL	=	Duration of Load
EMC	=	Equilibrium Moisture Conditions
MC	=	Moisture Content
MLP	=	Multi-Layer Perceptron
MLR	=	Multiple Linear Regression
RBF	=	Radial Basis Functions
RMSE	=	Root Mean Square
ROL	=	Rate of Loading
LogROL	=	logarithm of Rate of Loading

1 Introduction

Wood contains micro- or macro-voids that initiate crack propagation. A substantial amount of work has been done on fracture of wood and crack tip displacements (Patton-Mallory and Cramer 1987, Samarasinghe and Kulasiri 1998, 1999, 2000a, b, 2004, Samarasinghe et al. 2007, Bandara et al. 1999). However, very little has been done to understand fracture dynamics of wood, which includes time to crack initiation (T_{init}), duration of fracture (T_{frac}), time to catastrophic failure, load capacity associated with these events, and speed of crack propagation. The time to crack initiation and catastrophic failure are measures of the survival time of a member under load; therefore, how the presence of a crack influences time to failure is useful in the design of structures.

Nielsen (1978) defined two failure states in which 1) material damage starts or crack propagation is initiated, and 2) the damage level has reached a point where there is no load carrying capacity left and the rate of crack propagation increases catastrophically. The time to reach any of these failure states is said to be the corresponding time to failure. The first case is the lower limit of failure (safe mode) and the second case is the upper limit, or time to catastrophic failure. In this study, a detail investigation of time to crack initiation (T_{init}) and duration of propagation (T_{frac}) of a crack is made with respect to volume for three different ROL. Crack speed indicates the rate of propagation of a crack and it increases our knowledge of the energy dissipation mechanisms within the material. In this study, high-speed video imaging is used to look closely at these events.

Another important issue is that very little has been done to predict fracture toughness of individual wood samples from their own properties. Fracture of wood in relation to moisture content, temperature, density, and size has been studied separately (Porter 1964, Petterson and Bodig 1982). However, little is known about the combined effect of the size, ROL, physical variables, such as moisture content, density, and Young's Modulus, as well as geometric variables, such as grain angle, ring (face) angle and curvature of growth rings on fracture strength of a particular wood member. There is a considerable difference

in fracture toughness within the same species, pieces cut from the same tree and within the same batch of kiln dried wood. For these, it is typical to use the average fracture toughness. Therefore, it would be of much practical use, if load carrying capacity of *a particular cracked beam* can be predicted from its basic physical and geometric variables. Samarasinghe et al. (2007) demonstrated that properties of individual samples can explain the variation of fracture toughness and successfully predicted fracture toughness of individual samples of *pinus radiata* beams with a crack parallel to grain using neural networks. In this study, this work is extended to cracks perpendicular-to-grain.

Neural networks are powerful computational methods that enable the development of models that capture the underlying linear and nonlinear relationships between multitudes of variables. This study investigates the ability of Neural Networks to predict load carrying capacity of cracked beams from its size, ROL, and physical and geometric properties. If successful, it could provide a better method for predicting fracture strength of wood under the uncertain influence of physical and geometric variables than the currently used average values.

2 Objectives

The goal of this study was two fold: investigate fracture dynamics and model fracture toughness of individual wood beams with a sharp crack perpendicular to the grain. Its specific objectives were to:

- Study the time to crack initiation (T_{init}) and duration of crack propagation after initiation (T_{frac}) and their dependence on size and ROL,
- Use Neural Networks to analyse crack initiation and catastrophic loads from individual sample properties including volume, ROL, dry density, moisture content, Young's modulus, grain angle, face angle, and curvature of growth rings,
- Determine the speed of a propagating crack using high speed imaging and its relationship to ROL,
- Predict fracture toughness of individual samples from their physical and geometric properties using Neural Networks.

Fracture dynamics was an exploratory study and it was done on a subset of samples used for studying fracture toughness.

3 Background

3.1 Fracture Dynamics

From a study on duration of load (DOL) of solid wood beams under various ROL, Spencer (1978) found that although duration of load decreases with increasing loading rate, the 95th percentile held the load the longest and the 5th percentile held the load the shortest duration indicating the effects of strength reducing defects on DOL. However, how the rate of loading affects the time to fracture and failure of notched beams needs investigation. From experiments carried out on Douglas-fir, Mindness et al. (1978) showed that the initial crack speed, u, increases with the Mode-I fracture toughness, K_{Ic} as shown in Eq. 1:

$$\ln u = n \ln K_{Ic} + \ln A \tag{1}$$

where, A and n are positive constants.

3.2 Fracture Toughness

Fracture toughness is a measure of the strength of a cracked member and it uniquely defines the stress distribution surrounding a crack at the point of failure (Sih et al. 1965). Formulation of fracture theories assumes co-linear crack propagation. In most wood beams however, crack propagation is perpendicular to the existing crack (i.e. parallel-to-grain) and the associated fracture toughness is denoted by $K_{Ic(\mathrm{LT})}$ or $K_{Ic(\mathrm{LR})}$ where the original crack is perpendicular to grain and theoretical propagation direction is radial (R) or tangential (T).

Bending tests carried out on notched and solid specimens under various loading conditions have shown that the strength of solid beams increases with increasing ROL; however, the strength of notched beams remain unaffected by it (Madsen 1992). Spencer (1978) tested Douglas-fir solid

beams at 8 ROLs and found that the strength was insensitive to ROL up to about 50th percentile strength. However, the strength of higher percentiles increased with ROL and the effect was intensified as percentile increased towards the 95th percentile. In fact, Schniewind et al. (1978) found from creep studies on notched and knotty beams that fracture toughness increased with decreasing ROL thus eliminating the need for a load duration factor. Schniewind et al. (1978) further reports that Leicester (1974), who ramp tested notched beams to fail from 1 to 300 minutes, found the maximum fracture toughness for 30-minute duration.

As for size parameters, Stanzl-Tschegg et al. (1995) found from collinear crack propagation studies that the fracture toughness increased with net length (specimen length – crack length) and it also increased with thickness up to a point and then decreased. Barrett and Foschi (1978) found that K_{Ic} for cracks propagating along the grain in Douglas-fir specimens increased as thickness decreased. Similar increase in fracture toughness for thinner sections has been established for other materials due to plane stress conditions. Boatright and Garrett (in Patton-Mallory and Cramer 1987) used the variation in stress state across the crack front and the occurrence of irreversible deformation (cell buckling) to explain the higher K_{Ic} in thinner specimens. Johnson (1973) found that the variation of $K_{Ic(TL)}$ (cracks perpendicular to T direction and propagating in L direction) was insensitive to initial crack length and thickness. Porter (1964) found that the Mode-I critical strain energy release rate ($G_{Ic(TL)}$ and $G_{Ic(RL)}$) was independent of specimen length, thickness and height as well as crack length.

As for physical properties, Petterson and Bodig (1982) found that the fracture toughness ($K_{Ic(TL)}$) increased with specific gravity in the form of a power function and decreased with moisture content. Smith and Chui (1994) studied the effect of moisture content, density and the orientation (θ) of the original crack in the Radial-Tangential (RT) plane (measured as the angle between crack plane and tangent to a growth ring on the cross section) on critical strain energy release rate G_{Ic} of tensile specimens. They found that G_{Ic} increased from fibre saturation down to about 18% and then decreased with further decrease in moisture content slightly contradicting the continuous trend down to dry conditions found by Petterson and Bodig (1983). Smith and Chui (1994) state that the relationship between G_{Ic} and density becomes stronger as moisture content decreases.

Smith and Chui (1994) also found that G_{Ic} increased with decreasing θ down to 60° but decreased with further decrease in angle. Although the authors did not discuss the reasons for this trend, it can be explained as follows: when the angle is 90º, the crack plane coincides with the weak Longitudinal-Radial (LR) plane and therefore, a lower G_{Ic} can be expected. Similarly, when the angle is 0º, crack plane coincides with the Longitudinal-Tangential (LT) plane, which is also weak due to earlywood-latewood boundaries. Therefore, a lower G_{Ic} can again be intuited. Thus, the maximum G_{Ic} can be expected for an intermediate orientation of the crack plane as found by these investigators.

4 Artificial Neural Networks (ANN)

Neural networks are highly parallel computing methods that simultaneously analyse the interactions among many variables and therefore, are especially suitable for approximating nonlinear functions of many variables to any desired degree of accuracy (Samarasinghe 2006). A comprehensive introduction and a detailed coverage of neural networks are given in Samarasinghe (2006). Basic feed-forward networks, such as Multi-Layer Perceptron (MLP) and radial basis functions (RBF) networks, consist of an input, hidden, and output layers of neurons where MLP uses hidden neuron functions, such as linear, logistic, hyperbolic tangent etc. and RBF uses Gaussian functions. Each input neuron represents one input variable and the output neuron(s) represent the output variable(s). Connection strength between inputs and hidden layer neurons as well as hidden and output neurons are the free parameters of the network that need to be estimated starting with initial random values using an appropriate learning method until minimum prediction error is attained. The dataset is divided into training, testing and validation sets and these are used for training, testing the

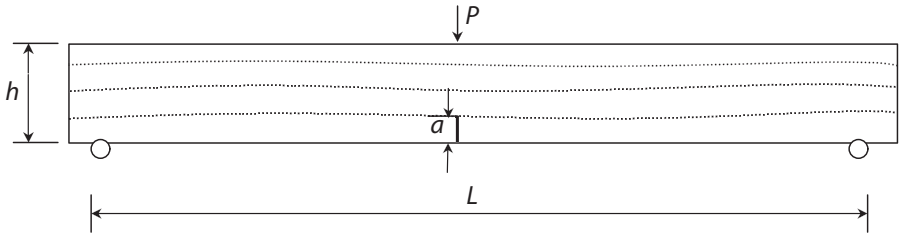

Fig. 1. Specimen with a crack perpendicular to grain. (*h* is height, *a* is crack length, *L* is span and *P* is applied load, patterns on the surface show grain orientation, and the two circles indicate the two rollers supporting the specimen).

accuracy while training, and validating the trained networks, respectively.

Seibi and Al-Alawi (1997) developed a feed-forward Multi-Layer Perceptron (MLP) Artificial Neural Network to investigate the effect of crack geometry, temperature and loading on fracture toughness of 7075-T651 aluminium alloy beams and plates containing surface and through-thickness cracks. Their model resulted in an R^2 value greater than 0.95 indicating that the network has captured a very strong relationship between the input variables and fracture toughness. They also used the developed ANN model to assess the contribution of individual input variables and found that temperature had a predominant influence followed by crack length to plate length ratio and crack depth to crack length ratio. They also found that the loading configuration, whether uni-axial or biaxial, played an insignificant role. Such sensitivity analysis in ANN is very useful for filtering variables that are significant for prediction. By using the developed model for analysing trends for scenarios not used in the training and testing of the ANN, the authors demonstrated the benefit of neural networks as an analytical tool.

Samarasinghe et al. (2007) successfully employed neural networks to predict fracture toughness of individual wood beams with an edge crack parallel-to-grain. In this study, the approach is extended to predict fracture toughness of individual wood beams with a crack perpendicular-to-the grain.

5 Methodology

5.1 Specimen Preparation and Testing Procedure

The specimens were prepared from kiln-dried boards cut from a log of New Zealand *pinus radiata* aged 30 years and especially bought for this research. Specimen configuration is shown in Fig. 1 and specimen dimensions are in Table 1 (*L* is span, *h* is height and *b* is thickness). There were 4 size categories (A, B, C, D) and each category had 51 specimens that were further divided into three sets for testing at three ROL. Specifically, 24 specimens were tested at 2.5 mm/min, 15 at 10 mm/min and 12 at 0.625 mm/min. There were a total of 204 specimens. The volume ratios for the specimens were 1 : 8: 64 : 297. The ROL ratios were: 1 : 4 : 16.

Cracks were made by first cutting a notch with a band saw and then sharpening it with a knife edge especially prepared for each specimen size in order to maintain the standard recommendation for crack length '*a*' : $0.45\,h \le a \le 0.55\,h$ where *h* is the height of beams. The maximum knife-edge cut was about 2 mm and the final crack length is shown in Table 1. The moisture content of specimens ranged from 4 to 16% that reflected the equilibrium moisture conditions (EMC) of a centrally heated building where the boards were stored prior to preparing specimens. These conditions were selected to simulate and study the effect of small variations in moisture content typical of wood used in interior conditions.

From the total batch of specimens, a subset consisting of 68 was used to record the entire crack propagation on a high-speed video camera

Table 1. Specimen sizes, rates of loading, geometric proportions, and sample sizes

Size category	Size ($L \times h \times b$) mm	No. of specimens for each ROL (mm/min) 2.5	10.0	0.625	Crack length (a) (mm)	a / h
A	1000 × 90 × 45	24	15	12	41	0.46
B	600 × 54 × 27	24	15	12	25	0.46
C	300 × 27 × 13.5	24	15	12	13	0.48
D	150 × 13.5 × 6.75	24	15	12	6	0.45

and their spread among the three loading rates for each of the four sizes was: 5 specimens for 10 mm/min, 8 for 2.5 mm/min, and 4 for 0.625 mm/min. These were used to explore fracture dynamics properties. Tests were carried out on a computer driven SINTECH (MTS) 30/D material testing machine. Four cylindrical load applicators were made, one for each size, according to ASTM standards for wood (1995) and a roller bed with adjustable spans were built to accommodate specimens with different spans as shown in Fig. 2. The supporting experimental resources were as follows: High-speed (450 frames/sec) video camera (HSC 250 × 2 of JC Labs Inc.), high speed recording device (SVHS Panasonic AG5700 video cassette and recorder) and a monitor, two light sources to illuminate the surface of the specimens and an electronic timer with a stop watch with an accuracy of 0.01 seconds.

The following is a description of the procedure used for high-speed video imaging of the process of crack propagation of the subset of 68 beams: The crack tip area was sprayed with black paint and the specimen was placed on the roller bed and the specimen surface was illuminated to obtain a clear image (Fig. 2). A graph paper was placed on the specimen and its image was recorded to calibrate the image distance to real distances. The timer was hung on the specimen closer to the crack and it was used to refer the images to load-time graphs obtained from the testing machine.

The load was applied at the rates specified in Table 1 and the high-speed camera was simultaneously activated. Video images of the specimen were recorded throughout the loading process until the specimen failed completely and 68 fracture processes were thus recorded. Load-deflection-time plots were also obtained from the testing machine to determine duration for crack initiation and catastrophic failure, and loads

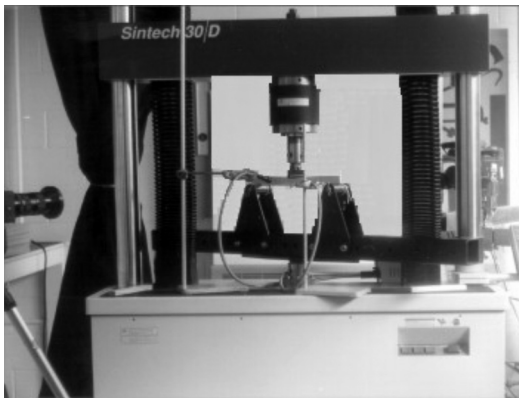

Fig. 2. Experimental set-up showing the specimen on the roller bed with adjustable span, light source with fibre optic cable (adjacent to specimen) and camera (on the left side of the image).

associated with these events. The investigations of time to failure and crack speeds were based on these specimens. The rest of the 136 beams were tested to failure in a similar fashion except that the crack propagation was not video recorded. For these, only the load-deflection plots were obtained. Total data set, however, was used for the study of crack initiation and catastrophic stresses and fracture toughness.

5.2 Physical and Geometric Variables

Data obtained for each specimen were: crack length, dimensions, density, moisture content, Young's modulus, ring angle, grain angle and curvature of growth rings. Soon after testing, two pieces near the tip were cut from every specimen to determine moisture content and dry density using the oven dry method (ASTM Standards-

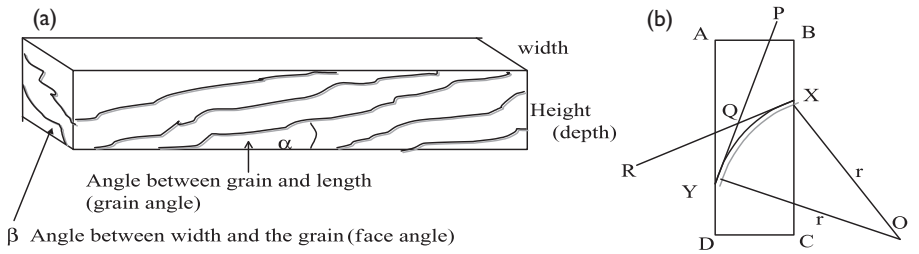

Fig. 3. Measurement of geometric properties: a) grain angle (α) and face angle (β) and b) curvature measurement (ABCD depicts the cross section, XY denotes section of growth ring whose curvature is measured, XR and YP are tangents to the growth ring and r is radius of the growth ring. Curvature was determined using these geometric parameters).

Wood 1995). Young's modulus for each cracked beam was estimated from a matched-sample cut from the adjacent material and tested in 3-point bending at the ROL specified for the corresponding cracked specimen. Tests were carried out using the same set-up used for testing cracked specimens; displacements were measured using images of the specimens and calibrated using an image of a graph paper set against each specimen prior to testing resulting in a resolution of 15.6 pixels/mm; and the load was obtained from the testing machine. Young's modulus was determined from the standard beam formula. Additionally, the grain angle (angle between grain and longitudinal axis of beam), face or ring angle (angle between width and tangent to a growth ring on the cross section), and ring curvature were measured as parameters affecting fracture and defining the subsequent crack path (Fig. 3). The range of the values for each variable was: moisture content (4–16%), grain angle (0.06° to 29°), face angle (0° to 80°), curvature (0.001 to 49.6), density (355 to 850 kg/m^3), and Young's Modulus (MOE) (7.71 to 12.24 GPa).

6 Results and Discussion

6.1 Some Experimental Observations

Following is a summary of some notable observations on crack initiation and propagation made from the tapes. Propagation in more than 40% of specimens did not start right from the existing crack tip indicating that any point in fracture process zone can reach the failure criteria and initiate crack propagation. All those cracks not originating from the tip subsequently joined the tip. In most of the specimens, cracks propagated along the grain. In few cases, a multitude of small cracks developed in different layers in the vicinity of the crack and fracture occurred in a staggered condition along some of these small cracks. Another feature observed was the crack extension and closure at high speeds where cracks propagate as a wave with oscillations which increased rapidly as the catastrophic failure was reached. A similar wave phenomenon was reported by Abraham (1997) for isotropic materials.

6.2 Time to Crack Initiation (T_{init}) and Propagation (T_{frac})

Typical load-time plots for the beams for all ROLs had an initial linear region, and at crack initiation graph became nonlinear. This time was recorded as the time to crack initiation and the corresponding load was recorded. Beyond crack initiation, load increases further up to the peak load at which point the load drops suddenly to pick up again and fail catastrophically at a later time. The variations were one in which peak load coincided with the catastrophic load and another in which load increased linearly up to the peak load. From each plot, the times to failure initiation and catastrophic failure as well as the crack initiation load and the peak load were obtained.

Time to crack initiation (T_{init}) was consistent in a predictable way for each volume and ROL. The T_{init} in relation to volume and ROL is shown in

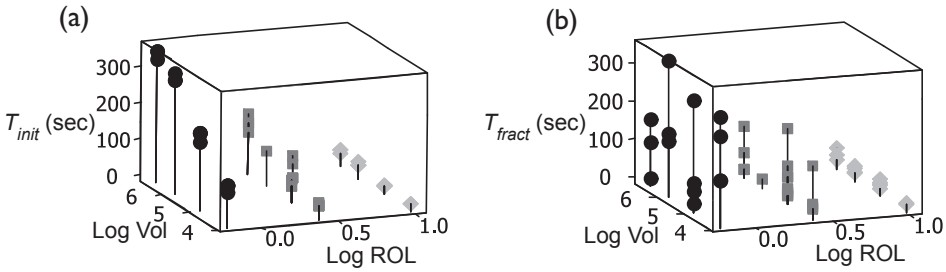

Fig. 4. Experimentally observed a) time to crack initiation (T_{init} – seconds) and b) duration of fracture (T_{frac}) in relation to volume and ROL. (Log Vol is logarithm of volume (mm^3) and Log ROL is logarithm of rate of loading).

Fig. 4a which shows that it is nonlinearly related to these two variables. For example, there is a pronounced effect of volume at the lowest ROL (0.625 mm/min). However, this effect diminishes as ROL increases and at the highest ROL (10 mm/min), the volume effect is almost negligible. As for the effect of ROL, Fig. 4a indicates that it is more pronounced on the largest volume that held the load disproportionately longer than the smaller ones. Table 2 displays the mean times to crack initiation and associated standard deviations (within brackets). Where there is no standard deviation, valid results could be obtained for only 1 out the four specimens.

In contrast to T_{init}, the duration of crack propagation (T_{frac}) was highly random as shown in Fig. 4b against volume and ROL (0.625, 2.5, 10 mm/min). Fig. 4b shows that once crack propagation has initiated, a beam can fail at any time regardless of the volume. However, it also shows that all specimens with the largest volume have failed relatively quickly at the lowest ROL. Table 2 shows the mean time to fracture and standard deviations (shown within brackets) which highlight the high variability of T_{frac} compared to T_{init}.

6.3 Stress at Crack Initiation and Peak Stress

Table 3 displays the mean and standard deviation of crack initiation and peak stresses (in MPa) with respect to specimen size and rate of loading. Fig. 5 shows the average initiation stress and peak stress against volume for the three ROLs and it indicates that the stresses follow a power function against volume. Statistical tests of significance based on two-sample t-tests showed no significant influence of ROL on both stresses at significance level of 0.05. However, volume effect was significant for crack initiation and peak stresses ($p < 0.001$) for all volumes.

6.3.1 Neural Network Predictions of Load Carrying Capacity

In establishing fracture toughness, it is crucial to have an accurate estimation of crack initiation load. ASTM guidelines indicate an acceptable limit for the ratio of crack initiation load to peak load as a measure of validity of a fracture test. Furthermore, Table 3 highlights a large variance of crack initiation stress within a size category (A, B, C, or D) compared to the variance of peak stress. Therefore, it would be useful if these can be estimated for an individual specimen from its own geometric and physical properties and test conditions (volume, ROL, density, moisture content, Young's modulus, grain angle, face angle, and curvature of growth rings) and study how they influence it. The statistics of the specimen properties are shown in Table 4 which indicates a fair amount of variation of these properties as well. Therefore, neural network models were developed to predict these stresses (and loads) from the above parameters. Results revealed that models predicting crack initiation load (P_{init}) and peak load (P_{peak}) produced much higher accuracy than those predicting the corresponding stresses; therefore, the following section presents models predicting P_{init} and P_{peak}, as accurate predictions

Table 2. Mean time to crack initiation (T_{init}), duration of fracture (T_{frac}) and associated standard deviations (shown within brackets) with respect to volume and ROL.

Sample size	ROL (mm/min)	Log(Vol) (mm^3)	T_{init} (sec)	T_{frac} (sec)
A (100×90×45)	0.625	6.61	341.67 (14.43)	82.95 (77.84)
A	2.500	6.61	125.00 (20.41)	41.10 (53.43)
A	10.000	6.61	32.71 (15.61)	36.65 (0.010)
B (600×54×27	0.625	5.94	306.66 (11.55)	204.17 (117.55)
B	2.500	5.94	78.33 (–)	6.30 (–)
B	10.000	5.94	22.40 (5.00)	9.92 (9.13)
C (300×27×13.5)	0.625	5.04	193.75 (12.5)	92.44 (123.83)
C	2.500	5.04	57.36 (29.46)	50.13 (59.03)
C	10.000	5.04	8.50 (1.00)	12.81 (10.88)
D (150×13.5×6.75)	0.625	4.14	95.00 (10.00)	176.01 (84.81)
D	2.500	4.14	24.00 (4.18)	36.45 (48.28)
D	10.000	4.14	5.00 (1.07)	2.31 (2.05)

Table 3. Crack initiation stress and peak stress and corresponding standard deviations with respect to specimen size and ROL.

Size mm^3	ROL mm/min	Crack init stress (MPa) mean	stdev	Peak stress (MPa) mean	stdev
A	0.625	7.94	4.10	17.64	2.30
1000×90×45	2.5	8.77	3.72	18.16	3.83
	10	8.49	4.86	17.74	3.67
B	0.625	9.97	3.86	21.65	2.79
600×54×27	2.5	10.33	8.05	25.51	3.82
	10	12.46	8.32	26.27	3.98
C	0.625	13.17	12.35	28.99	7.32
300×27×13.5	2.5	18.29	9.14	30.91	7.50
	10	19.66	11.61	33.01	7.86
D	0.625	35.39	11.93	55.56	8.23
150×13.5×6	2.5	46.09	16.05	65.02	14.40
	10	39.92	15.23	55.97	13.58

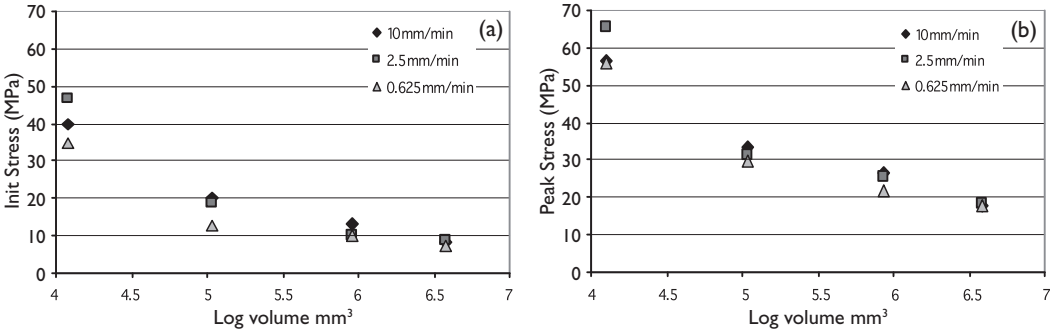

Fig. 5. a) Average crack initiation stress and b) average peak stress against volume for the three ROLs.

of load carrying capacity (whether load or stress) increases the accuracy of estimation of fracture toughness using the analytical formula.

For both models, the total data set was randomly divided into three sets – 60% for training, 20% for calibrating or testing the model during training and another 20% for validating the developed network. The validation set shows the prediction and generalization ability of the developed network when exposed to new data that it has not seen before. NeuroShell2 (1997) software was used to develop neural network models and a Multi-Layer Perceptron (MLP) network was the best model for predicting P_{init}. This neural network has one input layer, two sets of 8 neurons each in the hidden layer – with one set having Gaussian and the other set with Gaussian Complement activation functions-, and one output neuron with logistic activation. The network was trained with backpropagation with momentum and training was continued until the mean square error on the test set reached minimum.

Fig. 6 shows the actual and predicted load to crack initiation for the validation data set. Here, the prediction accuracy was such that the R^2 was 0.71 indicating that 71% of variability of P_{init} was captured by the inputs. Correlation coefficient between the predicted and actual loads was 0.85 and the root mean square (RMSE) on the validation data set was 0.125 (equivalent to 214 N). The order of the variables from the most to least significant and their contribution to predicting the crack initiation load as obtained from a sensitivity analysis, performed by analysing the influence of a variable while holding the other variables at their mean value, were: Log Volume (31%), Young's Modulus (16%), face angle (10.3%), moisture content (9.6%), curvature (9.2%), grain angle (8.3%), Log ROL (8.1%) and density (7.5%). For comparison, Multiple Linear Regression was also conducted on the data resulting in R^2 of 0.626, and RMSE of 0.135 (equivalent to 260 N).

As shown in Fig. 5b and Table 3, peak stress for all 204 specimens was more consistent. Similar observation was made for peak load by Boontanjay (1979) for notched *pinus radiata* beams. Neural networks were developed to predict peak load for individual cracked beams from their physical and geometric properties and test conditions. The best network was an MLP network with

Table 4. Statistics of physical and geometric properties of specimens.

	Min	Max	Average	St.dev
Moisture content (%)	4.1	16.0	10.3	1.51
Grain Angle (rad)	0.001	1.222	0.102	0.147
Face Angle (rad)	0.001	1.57	0.724	0.475
Curvature	0.001	49.6	8.78	9.81
Dry Density (kg/m^3)	355	850	482	63.5
Young's Mod. (GPa)	7.71	12.24	8.64	2.55

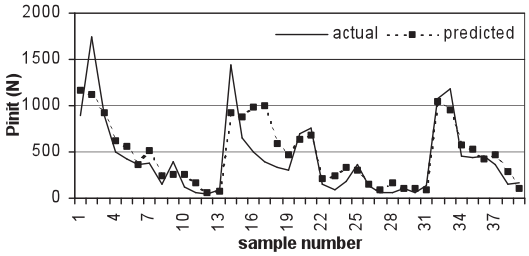

Fig. 6. Experimental and Neural network predicted crack initiation load P_{init} (validation data). (N indicates Newtons)

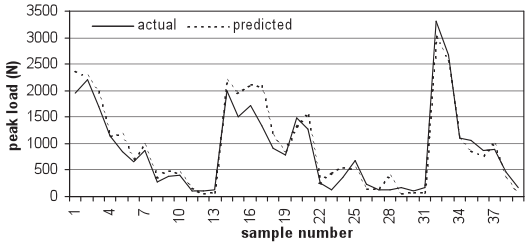

Fig. 7. Experimental and Neural Network predicted peak load (validation data).

2 sets of 8 hidden neurons with one set having Gaussian and the other with Gaussian complement activation functions, and one output neuron with logistic activation. Fig. 7 shows the peak load predicted from the neural network and the actual load for the validation data set that produced an R^2 value of 0.918 (91.8% of variability captured by the inputs), correlation coefficient of 0.968 between the predicted and actual loads and RMSE of 0.086 (equivalent to 222 N). It shows high prediction accuracy indicating that the neural network has captured the variation in the peak load extremely well. A sensitivity analysis revealed the following order of significance and contribu-

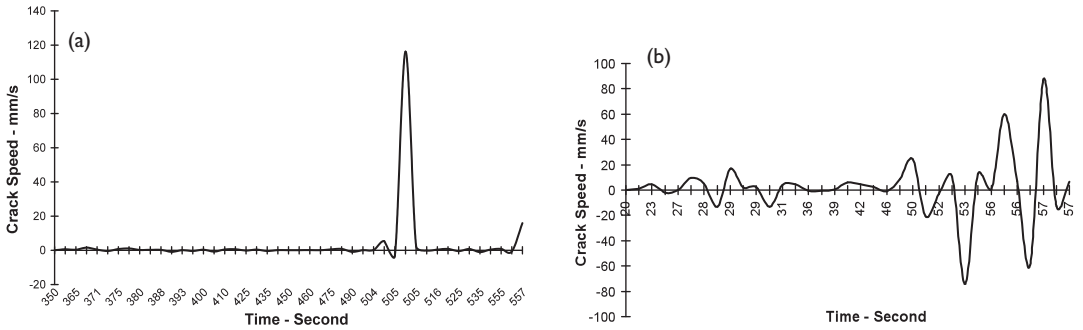

Fig. 8. Crack speed profiles for the largest volume for ROL of: a) 0.625 mm/min and b) 10 mm/min.

tion of the variables to the peak load: log volume (28.4%), Young's modulus (14%), density (13%), grain angle (11.9%), moisture content (11.3%), curvature (8.7%), Log ROL (6.9%), and face angle (6.0%). Some variables have reversed the order of significance from the crack initiation load analysis but Young's modulus appears to be the most important secondary variable for both peak and crack initiation loads. For comparison, MLR was conducted and the resulting R^2 was 78.4% and RMSE was 0.122 (equivalent to 395 N).

6.4 Crack Speed Profiles

This section investigates speed of crack propagation in the beams in relation to ROL. The fracture process of the 68 specimens selected for monitoring crack propagation were recorded on 3-hour SVHS videotapes resulting in 9 hours worth of information. One of the drawbacks in the use of the digitized video images was the hard disk space required to store them. For example, 2–3 minute duration of video occupied about 100 MB space. Therefore, important still images, between 20–100 images along with the graph scale image per specimen, were captured from the tapes at appropriate events using Vedium Movie Clip multimedia imaging software and relevant hardware (1998). Graph scale was used to convert image pixel distances to mm. For a digital image, the smallest unit is called a pixel, or picture element, and the image size in this study was 512×512 pixels. The crack length over time was computed using the crack tip coordinates obtained at the beginning and end of a specified time period. The crack speed during the same time period was calculated by dividing the crack length by the time interval.

Fig. 8a and b show crack speed profiles within the time duration of fracture for two typical specimens of the largest size A (1000×90×45) for the minimum and maximum ROL tested. Fig. 8a shows that the crack speed is very low at the lowest rate (0.625 mm/min) up to the catastrophic failure state where crack speed jumps rapidly in the form of a spike up to about 120 mm/sec. This indicates slow and stable crack propagation until catastrophic failure. At the highest rate of loading (10 mm/min) however, speed fluctuates significantly throughout the fracture process with oscillations with an overall increase up to the catastrophic failure where speeds of about 100 mm/sec are reached (Fig. 8b). This profile indicates a fast and turbulent mode of crack extension at the highest ROL.

The negative speeds indicate crack closure where crack lips touch each other, and it was predominant in the vicinity of the catastrophic failure. Nielsen (1978) used an assumption of non-negative crack speeds in the time interval between crack initiation and catastrophic failure to derive expressions for the time to catastrophic failure. According to our study however, alternate negative and positive speeds were quite frequent and negative speeds are reasonably high in many cases and quite significant for the highest ROL. The speed profiles for the other two sizes are not ready due to the labour and time intensive extraction of data from the digitized images. Therefore, the size effect on crack speed is not studied at this point.

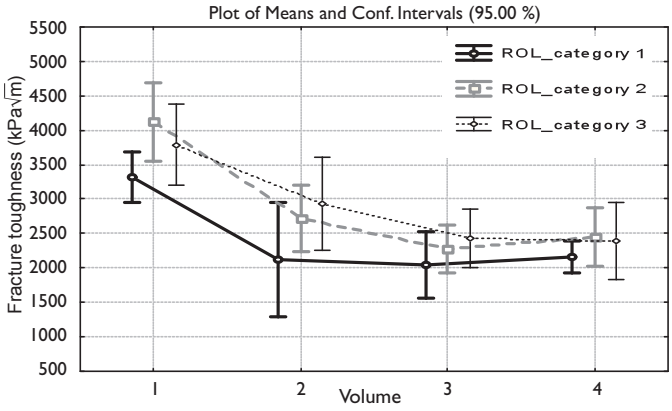

Fig. 9. Fracture toughness in relation to volume and ROL.

6.5 Predicting Fracture Toughness of Individual Samples Using Neural Networks

The inconsistency of the crack initiation load prominently displayed in this study resulted in the ratio of peak load to crack initiation load ranging from 1 to 5.6. For metals, ASTM standards (1995) recommended ratio is 1.1 for a mostly linear load-displacement plot up to failure. In wood beams, there is a large nonlinear region before failure and therefore, the ratio adopted for metals is not suitable. Boontanjay (1979), who tested notched *pinus radiata* beams, also found a large ratio and he arbitrarily selected 2.5 as the maximum acceptable ratio for a valid fracture toughness test. In our study, a ratio of 2.5 was selected and this reduced the data set to 72% of the original set. We noted that the large ratios were more a characteristic of larger volumes. For example, the rejection rate from the largest to smallest volumes was: 31%, 38%, 18%, and 4%. For the reduced set, the fracture toughness (K_{Ic}) was obtained from the standard formula and associated correction factor (Pilkey 1994) given below:

$$K_{Ic} = \frac{6P_{init}L}{4bh^2}\sqrt{\pi a}\,F\left(\frac{a}{h}\right) \quad (2)$$

$$F\left(\frac{a}{h}\right) = 1.106 - 1.552\left(\frac{a}{h}\right) + 7.71\left(\frac{a}{h}\right) - 13.53\left(\frac{a}{h}\right)^3 + 14.23\left(\frac{a}{h}\right)^4 \quad (3)$$

where, a is crack length, h is height (Fig. 1) and b is width (thickness) of the specimen, L is span, and Pinit is load at crack initiation. Fig. 9 shows the relationship between fracture toughness and volume (1 indicates the smallest and 4 the largest) for the three ROLs (1 indicates the smallest and 3 the largest) in terms of mean and 95% confidence intervals. The figure shows that the fracture toughness is the largest for the smallest volume and its sensitivity diminishes for larger volumes.

Statistical tests of significance using two sample t-tests indicated that the ROL effect on mean fracture toughness was insignificant for all volumes at $\alpha = 0.05$. With regard to sample size, statistical t-tests indicated that the mean fracture toughness of the smallest volume was significantly different from that for the three larger volumes at α level of 0.05.

Simple linear correlation analysis conducted on STATISTICA (2007) indicated statistically significant correlations ($p < 0.05$) between fracture toughness and: LogVolume (–0.517), Young's modulus (0.405), face angle (–0.443) and grain angle (–0.244), and statistically insignificant correlation between fracture toughness and: curvature, dry density, moisture content and LogROL. Since these were linear correlation coefficients, they do not capture nonlinear effects typical of wood, which ANN are capable of capturing. Therefore, all variables were included in the model development.

NeuroShell (1997) and STATISTICA (2007)

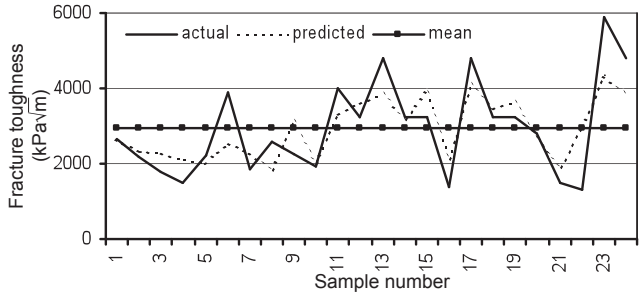

Fig. 10. Observed and predicted fracture toughness with superimposed mean value.

that tests a variety of network architectures and activation functions in MLPs and Radial Basis Functions (RBF) while also testing them on subsets of inputs were used to train 10 networks using several learning methods including backpropagation with momentum, quickprop, and conjugate gradient methods. The 5 top performing networks were selected based on R^2, RMSE and correlation between the predicted and actual data and, out of these, the best was an MLP network with two sets of 6 hidden neurons, one set with logistic and the other with Gaussian complement and an output neuron with logistic activation and using all 8 inputs. This model produced an R^2 of 0.62 on the validation data indicating that 62% of variability of K_{Ic} is explained by the input variables. The correlation coefficient between actual and predicted values was 0.813 ($p<0.05$), and RMSE was 0.0961 (equivalent to 532 kPa$\sqrt{m}$).

The other four networks used all inputs and were inferior to this model but had similar performance to each other with statistically significant ($p<0.05$) correlation coefficient between the actual and predicted output ranging from 0.542 to 0.593. These were: 3 RBF functions with 26, 22, and 20 hidden neurons and an MLP network with 12 hidden neurons with tanh activation functions in hidden and output layers. The RMSE for these networks based on the validation dataset that was not used in model development were, 0.138, 0.137, 0.131, 0.133 and 0.141, respectively. Fig. 10 shows a plot of the relationship between the actual and predicted fracture toughness from the best model on validation data along with the mean fracture toughness depicted by the horizontal line. A multiple linear regression (MLR) model produced an R^2 of 0.297 and RMSE of 0.178 which is inferior to results from all neural networks indicating the presence of nonlinear relationships not captured by MLR.

Fig. 10 shows that the predicted values for most specimens are better than the mean value indicating the advantage of predicting fracture toughness from individual specimen properties. Considering the constant values generally assumed for fracture toughness properties of a single species in dry conditions, these results are encouraging. Samarasinghe et al. (2007) also showed that even for the same kiln-dried batch, meaningful relationships can be found between K_{Ic} and individual specimen properties.

The developed neural network was also subjected to sensitivity analysis to find the relevance of the input variables. This was done by removing one variable at a time from the model and determining the increase in error in model prediction when this variable was unavailable. The results indicated that the most to least influential variables and their contribution to predicting fracture toughness were; LogVolume (28.3%), Young's modulus (12.7%), LogROL (12.6%), density (10.4%), moisture content (10.1%), face angle (9.5%) and curvature (8%). Although the mean fracture toughness values were statistically insignificant with respect to LogROL, it shows an influence for individual specimens.

7 Summary and Conclusions

This study explored fracture dynamics properties of cracked wood beams of four sizes. The volume and ROL interact nonlinearly affecting time to crack initiation. For example, the volume effect was more marked at the smallest ROL where the largest volume held the load a disproportionately longer time. However, the volume effect was negligible at the largest ROL. The time to crack initiation was consistent; in contrast, the time to crack propagation was more variable for a particular size category. However, at the lowest ROL, the largest volume failed more quickly after crack initiation. The crack propagation was a wave phenomenon leading to negative (crack closure) and positive speeds, especially at the highest ROL, reaching very high speeds at the catastrophic failure.

Both the average crack initiation and peak stresses were insensitive to ROL but were significantly affected by volume. However, the peak stress was more consistent than the crack initiation stress. Neural network models were developed successfully to predict both the crack initiation and peak loads for individual samples from their physical and geometric variables including volume, rate of loading (ROL), Young's modulus, density, moisture content, grain angle, curvature of growth rings and face angle. Both showed strong correlations and high predictability resulting in R^2 of 0.71 and 0.918, respectively, and correlation coefficients between the actual and predicted load of 0.85, and 0.968, respectively. These models indicated that volume was the predominant variable and Young's modulus was the most important secondary variable affecting initiation and peak loads. Other variables showed varying contributions to the two loads.

The mean fracture toughness was insensitive to ROL and there was a significant difference between the mean fracture toughness of the smallest volume and that of the other three volumes. The best neural network model developed to predict toughness of each individual beams produced an R^2 of 0.62 and correlation coefficient of 0.813 between the predicted and actual values.

The study showed that the neural networks can predict crack initiation load, peak load and fracture toughness of individual beams from their properties and are useful for assessing their contributions. The predicted fracture toughness was significantly better than the mean value. As crack initiation load could be predicted successfully, in future, it may be possible to use crack initiation load predicted from easily measurable properties of individual specimens to calculate fracture toughness. Alternatively, the model developed to estimate fracture toughness directly can be used. The current study dealt with only a limited range of values for the variables representing interior use of kiln-dried wood based on specimens derived from one log. However, it is promising that with a larger database representing a larger range of values, neural networks have the potential to predict load capacity of cracked members under the uncertain influence of physical and geometric variables.

References

Abraham, F.E. 1997. Portrait of a crack; rapid fracture mechanics using parallel molecular dynamics. IEEE Computational. Sciences and Engineering 4: 66–77.

ASTM Standards-Metal testing. 1995. E 1290-section 1290. p. 869.

ASTM Standards-Wood. 1995. D 143.

Bandara, D.M., Samarasinghe, S. & Mackenzie, D.W. 1999. High-speed video imaging to study effect of volume and speed of testing on fracture dynamics of wood. Proc. of Pacific Timber Engineering Conference, Rotorua, New Zealand. p. 300–307.

Barrett, D. & Foschi, R.O. 1978. On the application of brittle fracture theory, fracture mechanics and creep-rupture models for the prediction of the reliability of wood structural elements. Proc. of the First International Conference on Wood Fracture, Forinteck Canada Corp., Vancouver, Canada. p. 1–37.

Boontanjay, C. 1979. Fracture toughness of New Zealand pinus radiata. ME Thesis, University of Auckland, New Zealand.

Johnson, J.A. 1973. Crack initiation in wood plates. Wood Science 6(2): 151–158.

Madsen, B. 1992. Structural behaviour of timber. Timber Engineering Ltd. Vancouver, Canada. 440 p.

Mindness, S., Madison, B. & Barrett, J.D. 1978. Rate of loading and duration of load tests on Douglas-fir in tension perpendicular to the grain. Proc. First International Conference on Wood Fracture, Forinteck Canada Corp., Vancouver, Canada. p. 143–157.

NeuroShell 2. 1997. Ward Systems Group, Inc., Frederick, Maryland, USA.

Nielsen, L.F. 1978. Crack failure of dead-, ramp-, and combined-loaded viscoelastic materials. Proc. First International Conference on Wood Fracture, Forinteck Canada Corp., Vancouver, Canada. p. 187–200.

Patton-Mallory, M. & Cramer, S. 1987. Fracture mechanics: a tool for predicting wood component strength. Forest Products Journal 37(7/8): 39–47.

Petterson, R.W. & Bodig, J. 1982. Prediction of fracture toughness of conifers. Wood and Fiber Science 15(4): 302–316.

Pilkey, W.D. 1994. Formulas for stress strain and structural matrices. Chapter 7. Linear Elastic Fracture Mechanics Applications. John Wiley & Sons. USA.

Porter, A.W. 1964. On the mechanics of fracture in wood. Forest Products Journal 14: 325–331.

Samarasinghe, S. 2006. Neural Networks for applied sciences and engineering – from fundamentals to complex pattern recognition. Taylor & Francis, Florida, USA.

— & Kulasiri, D. 1998. Investigation of stress intensity factors of wood using image processing and orthotropic fracture theory. Proc. of 12th Engineering Mechanics Conference, La Jolla, USA. p. 618–621.

— & Kulasiri, D. 1999. Fracture toughness of wood based on experimental near-tip displacements and orthotropic fracture theory. Proc. of Pacific Timber Engineering Conference, Rotorua, New Zealand. p. 292–299.

— & Kulasiri, D. 2000a. Displacement fields of wood in tension based on image processing: Part 1. Tension parallel- and perpendicular-to-grain and comparisons with isotropic behaviour. Silva Fennica 34(3): 251–259.

— & Kulasiri, D. 2000b. Displacement fields of wood in tension based on image processing: Part 2. Crack-tip displacements in Mode-I and Mixed Mode fracture. Silva Fennica 34(3): 260–273.

— & Kulasiri, D. 2004. Stress intensity factor of wood from crack-tip displacement fields obtained from digital image processing. Silva Fennica 38(3): 267–268.

— , Kulasiri, D. & Jamieson, T. 2007. Neural networks for predicting fracture toughness of individual wood samples. Silva Fennica 41(1): 105–122.

Schniewind, A.P., Bartels, H.J. & Gammon, B.W. 1978. Effect of pre-loading on fracture toughness of wood. Proc. of 1st International Conference on Wood Fracture, Forinteck Canada Corp., Vancouver, Canada. p. 227–238.

Seibi, A. & Al-Alawi, A.M. 1997. Neural Networks for predicting fracture toughness in metals. Engineering Fracture Mechanics 56(3): 311–319.

Sih, G.C., Paris, P.C. & Irwin, G.R. 1965. On cracks in rectilinearly anisotropic bodies. International Journal of Fracture Mechanics 1: 189–203.

Smith, I. & Chui, Y.H. 1994. Factors affecting mode I fracture energy of plantation-grown red pine. Wood Science and Technology 28(2): 147–157.

Spencer, R.A. 1978. Rate of loading effect of bending for Douglas-fir. Proc. of 1st International Conference on Wood Fracture, Forinteck Canada Corp., Vancouver, Canada. p. 259–280

Stanzl-Tschegg, S.E., Tan, D.M. & Tschegg, E.K. 1995. New splitting method for wood fracture characterization. Wood Science & Technology 29: 31–50.

STATISTICA 2007. StatSoft Inc., Tulsa, Oklahoma, USA.

Total of 29 references